Transactions in GIS

Research Article

*Transactions in GIS*, 2013, ••(••): ••–••

# Airborne LiDAR and Terrestrial Laser Scanning Derived Vegetation Obstruction Factors for Visibility Models

Jayson Murgoitio,* Rupesh Shrestha,† Nancy Glenn† and Lucas Spaete†

*Bureau of Land Management, Boise, Idaho
†Department of Geosciences, Idaho State University

**Abstract**

Research presented here explores the feasibility of leveraging vegetation data derived from airborne light detection and ranging (LiDAR) and terrestrial laser scanning (TLS) for visibility modeling. Using LiDAR and TLS datasets of a lodgepole pine (*Pinus contorta*) dominant ecosystem, tree canopy and trunk obstructions were isolated relevant to a discrete visibility beam in a short-range line-of-sight model. Cumulative obstruction factors from vegetation were compared with reference visibility values from digital photographs along sightline paths. LiDAR-derived tree factors were augmented with single-scan TLS data for obstruction prediction. Good correlation between datasets was found up to 10 m from the terrestrial scanner, but fine scale visibility modeling was problematic at longer distances. Analysis of correlation and regression results reveal the influence of obstruction shadowing inherent to discrete LiDAR and TLS, potentially limiting the feasibility of modeling visibility over large areas with similar technology. However, the results support the potential for TLS-derived subcanopy metrics for augmenting large amounts of aerial LiDAR data to significantly improve models of forest structure. Subtle LiDAR processing improvements, including more accurate tree delineation through higher point density aerial data, combined with better vegetation quantification processes for TLS data, will advance the feasibility and accuracy of data integration.

## 1 Introduction

Visibility models are important for a wide range of applications, such as transportation safety, homeland security, real estate, and land use planning. Incorporating vegetation into visibility models is important in order to understand how visibility patterns are affected by vegetation (Llobera 2007). Vegetation obstructions have been factored into visibility models using a variety of techniques and algorithms, including probabilistic models (Fisher 1992, Ogburn 2006, Standford et al. 2003), models of visual permeability (Dean 1997), three dimensional obstruction representation (Liu et al. 2008), and the Beer-Lambert Law of Attenuation (Bartie et al. 2011, Llobera 2007). Despite these and other studies, no framework has been presented which incorporates actual three-dimensional forest vegetation data into short-range visibility models and that has been tested with systematic and objective accuracy assessment methods.

Data acquisition and quantification of vegetation elements for use as obstruction variables in visibility models is difficult, especially in large areas of stochastic forested environments. Recent advancements in light detection and ranging (LiDAR) have provided a viable method

**Address for correspondence:** Nancy F. Glenn, Department of Geosciences, Idaho State University, 322 E. Front St. Suite 240, Boise, ID 83702, USA. E-mail: glennanc@isu.edu

Acknowledgements: This work was supported by the NSF Idaho EPSCoR Program and by the National Science Foundation under award number EPS-0814387, NSF EAR-1226145, and NOAA OAR Earth Systems Research Laboratory/Physical Sciences Division (ESRL/PSD) Award NA09OAR4600221. LiDAR data for this project was generously shared by the University of Idaho, supported by the NSF Idaho EPSCoR Program.



doi: 10.1111/tgis.12022

for quantifying vegetation structures (Lefsky et al. 2002). Several studies have demonstrated the ability of airborne LiDAR for delineating tree location (Chen et al. 2006, Ke and Quackenbush 2008, Persson et al. 2002, Wang et al. 2008), modeling canopy characteristics (Coops et al. 2007, Popescu and Wynne 2004), and determining tree structure (Hall et al. 2005, Lefsky et al. 2005, Richardson et al. 2009). However, the vertical perspective, narrow off-nadir incidence angle (± 20°) and relatively low pulse density (<20/m$^2$) of aerial LiDAR hinders the amount and accuracy of data obtained from subcanopy tree structure (Zimble et al. 2003). For many forestry applications, such as large-scale estimation of biomass, these lower structural elements are typically estimated from aerial LiDAR returns dispersed vertically through the canopy (Ni-Meister et al. 2001). Modeling visibility at ranges of less than a few hundred meters, however, requires higher precision structural information of vegetation obstruction, especially of subcanopy tree elements (Murgoitio et al. 2013).

Aerial LiDAR has been successfully used to model tree trunk obstructions into visibility analysis, but was not found as effective in modeling subcanopy structure (Murgoitio et al. 2013). Terrestrial laser scanning (TLS), which provides a lateral perspective and generates denser point clouds, can augment airborne LiDAR as a source of high resolution subcanopy structural information (Chasmer et al. 2006, Henning and Radtke 2006). We hypothesize that the combination of vertical and lateral data is advantageous for incorporating vegetation influences on short-range visibility models. Similar to the canopy shadowing shortcoming of aerial LiDAR, the lateral perspective of terrestrial LiDAR can be obstructed by vegetation instances. As a result, typical TLS collection schemas include scans from multiple locations, which are subsequently combined to extract high resolution information over a relatively small area.

Integration of aerial and terrestrial data for estimation of full vertical forest canopy structure has not been widely explored, especially over large areas (Chasmer et al. 2006). Moskal et al. (2009) highlights the potential of synergizing point clouds for analysis of calculation of canopy volume and diameter at breast height, but does not fully address large-scale fusion of TLS and aerial data. Other research that uses TLS data for augmentation of aerial LiDAR has largely been limited to urban environments, with data utilized to integrate man-made structures into surface models (Böhm and Haala 2005). Similarly, Bartie et al. (2011) acknowledge the potential of TLS as a supplement to aerial LiDAR delineation of tree metrics in an urban environment, but do not attempt to integrate terrestrial data.

Once data have been fused, the subsequent challenge is applying TLS and LiDAR-derived vegetation obstructions together in a practical process for predicting visibility. Previous studies which factor vegetation into visibility models have established a potential methodology and framework for incorporating remotely sensed data. Dean (1997) utilized a series of triangular irregular networks to hold values of visual permeability through vegetation, calculating visibility as a function of the distance a sightline traverses through vegetation instances. Dean's method was improved upon with a model by Llobera (2007), who hypothesized that visual permeability could be calculated through a function of the Beer-Lambert law. This improved model considers a beam of light, or vision, projecting down a sightline path from an observer towards a target. The beam attenuates with each instance of vegetation, proportionate to the number, length, and relative amount of occlusion encountered. While Llobera used synthetic data to demonstrate the Beer-Lambert modeling method, Bartie et al. (2011) incorporated these principles within a visibility model of urban environments with vegetation factors, calculating tree characteristics from a combination of aerial LiDAR and multispectral imagery. Bartie's method demonstrated that although instances and relative lengths of vegetation within the sightline beam could be readily identified with aerial LiDAR, the density metric required further refinement.

 

Previous research used aerial LiDAR derived individual tree trunks as an input variable to improve visibility models within a forested environment (Murgoitio et al. 2013, Murgoitio, 2012). These studies used airborne LiDAR data to model tree trunks as obstructions into the visibility model in ArcGIS and found that the accuracy of the visibility model improved to 91.2% compared with the accuracy ranging from 34.3% (without vegetation) to 68.9% (with vegetation) using traditional viewshed models. The research presented herein further refines the visibility analysis by incorporating sub-canopy obstructions (such as branches and needles) using both TLS and aerial LiDAR data. The goal was to determine whether TLS and LiDAR-derived tree characteristics could be practically associated with distance for visibility analysis. Our approach surmised that if a relationship between forest characteristics relative to visibility derived from aerial LiDAR and TLS was found, a density metric could be applied to broad areas of aerial LiDAR data for modeling visibility. To explore this relationship, we systematically established a percentage of sightline visibility derived from digital photography at predefined distance intervals. Next, we used aerial LiDAR to delineate individual tree location, canopy area, and height to search for a practical relationship between tree characteristics and sightline visibility. Finally, tree data derived from LiDAR was compared with TLS-generated density values to explore the relationship between vertical and lateral perspective datasets relevant to visibility models.

## 2 Methods

### *2.1 Study Area*

This study was situated in the Challis National Forest of Central Idaho, approximately 18 km west of Stanley, Idaho, USA (114° 56′W, 44° 13′N). The study area is characterized by a homogenous lodgepole pine (*Pinus contorta* Dougl. ex Loud.) forest, aged 80 to 120 years, with minimal underbrush (Steele et al. 1981) and ranges from approximately 1,990 to 2,030 m above sea level. The terrain consists of rolling hills interspersed with riparian areas and meadows along streams and low lying areas. A total of 15 study plots were randomly selected from flat terrain (slope of $\leq 2\%$) within the footprint of the airborne LiDAR data. Flat terrain was sought to minimize the effect of ground topography, such as visibility shadowing by hills. At these 15 plots, field samples of digital photography were collected to compare LiDAR derived vegetation obstructions. Four of the plots were scanned with a TLS for extraction of subcanopy tree structure information (Figure 1).

### *2.2 Field Collection*

Field data collection occurred on June 28–30, 2011. Each study plot was centered on a single observation point, with three 50 m transects extending outward at random azimuth values from 1–360°. Observation and end points were georeferenced with a Topcon GR-3 RTK survey-grade GPS unit, capable of 0.3 cm and 0.5 cm horizontal and vertical error, respectively (Topcon Positioning Systems Inc., Livermore, CA). A 1 $m^2$ target, constructed of wood and orange cloth, centered at 1.37 m (4.5 ft) above ground level, was then positioned at 5 m sampling intervals along the 50 m sightline. A digital photograph was taken of the target at each interval with the camera positioned directly above the observation point at a height of 1.37 m above ground level using a tripod.

A total of 450 individual locations were sampled. Of these, 406 images were acquired to calculate target visibility and the remaining 44 samples were assessed as completely obstructed

 

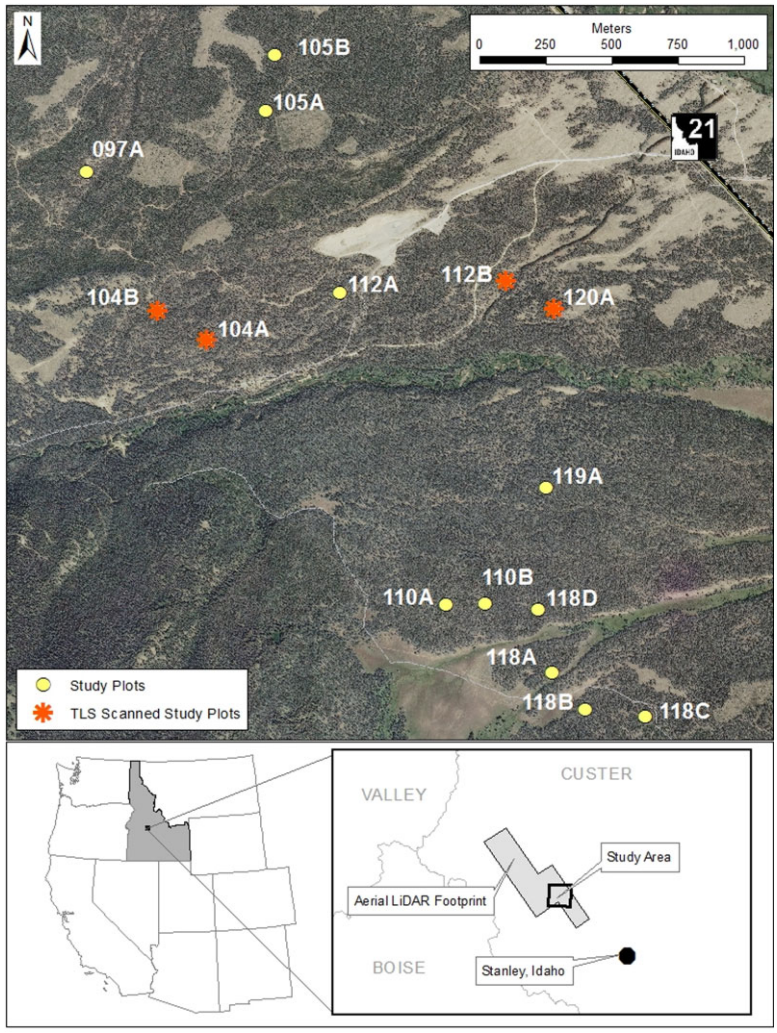


**Figure 1** Map of study area, Challis National Forest, Custer County, Idaho, USA

during field collection. Using known values of camera resolution, lens field of view, and image focal length, a total pixel count for the full 1 $m^2$ target was calculated for each image, and used to assess proportion of the visible target area. The photographs were used to isolate tree trunks and provide a proportion of target visibility attributable to trunk obstructions using the method described in Murgoitio et al. (2013). The visibility established from this process (referred to hereafter as 'reference visibility') provided a metric of target obstruction that could be directly and easily related to binary visibility calculations at defined spatial intervals.

### *2.3 LiDAR Data*

Watershed Sciences Inc. (Portland, OR) collected aerial LiDAR data on August 4–5, 2010 using a Leica ALS50 Phase II discrete LiDAR sensor (Leica Geosystems, Heerbrugg, Switzer-

 

land) mounted in a Cessna Caravan 208B. The sensor system collected data at 900 m above ground level, with a pulse rate of ≥83 kHz. Individual flight lines were overlapped ≥ 50% with a scan angle of ±13° from nadir. Vendor reported vertical accuracy was 3.28 cm with an overall first return point density of 8.68 points $m^{-2}$.

Aerial LiDAR data were processed in Environment for Visualizing Images (ENVI; Exelis, Boulder, CO) version 4.8 using the BCAL LiDAR Tools developed by the Idaho State University's Boise Center Aerospace Lab (BCAL) (http://bcal.geology.isu.edu/envitools.shtml, Streutker and Glenn 2006). To separate ground and vegetation returns, LiDAR point cloud data were height filtered using the BCAL LiDAR Tools. The height filtering uses the lowest elevation points within a user-defined moving window (or canopy spacing) to create a surface using interpolation parameters. The points that are below the surface are classified as ground points and iteratively added to re-create the surface until no more unclassified points are below the surface. A 7 m canopy spacing and a natural neighbor interpolation was used to height filter the point cloud data. Using the BCAL LiDAR Tools, the height filtered point cloud data were subset in 60 m radius sections centered on the observation points, and raster datasets with a resolution of 0.2 m for bare earth and mean vegetation height were derived for each study plot.

The 0.2 m resolution LiDAR-derived vegetation height raster of each study plot was used to delineate individual tree crowns using a multi-resolution segmentation followed by a region growing approach in Trimble eCognition® Developer version 8.6 (Trimble Geospatial, Westminster, CO) (Murgoitio et al. 2013). Lodgepole pine canopies are typically an elongated conical shape, with long, straight trunks with a slight taper (Steele et al. 1981). We assumed that the apex of the canopy corresponded with the trunk location on a straight vertical line to the forest floor. While aerial LiDAR has been shown to accurately measure tree heights within 1 m (Hyyppa et al. 2004, Kwak et al. 2007), the average point density of the discrete data (8.68 $m^{-2}$) meant that the single highest canopy return may not necessarily be from the tree apex (Chasmer et al. 2006). Instead, the centroid of the treetop polygon, delineated in eCognition with a raster surface, was designated as the location of the tree trunk for spatial calculations.

### *2.4 Terrestrial Laser Scanning Data*

TLS data were collected on four study plots within the aerial LiDAR footprint using a Leica ScanStation C10® system (Leica Inc., Heerbrugg, Switzerland). All scans were completed using a 360° horizontal and 90° vertical field-of-view with a resolution producing a surface precision of <2 mm at 50 m. The pulse diameter was 4.5 mm at sensor and 50 m with minimal effect from beam divergence. Array resolution was <2 mm, with estimated distance accuracy of a single pulse at 50 m at 4 mm or better. Scan locations were set over the same georeferenced observation points as were used for digital image acquisition, with single control points marked and delineated using RTK GPS. Scanner heights were set at 1.37 m above ground level which corresponded with camera height used for digital image acquisition.

TLS data processing was performed in Leica Cyclone® software. Scanner, control, and sightline endpoint locations were imported into the software to georeference each scan for integration with aerial LiDAR data. TLS data were then subset for comparison with reference visibility calculated from digital imagery. First the TLS point cloud was sliced horizontally to create a 1 m thick disk of TLS data centered at the scanner location and 1.37 m above the sightline endpoint location. This horizontal disk included all the points from 0.87 m to 1.87 m height from the ground surface. Next, viewing the point cloud from a top

 

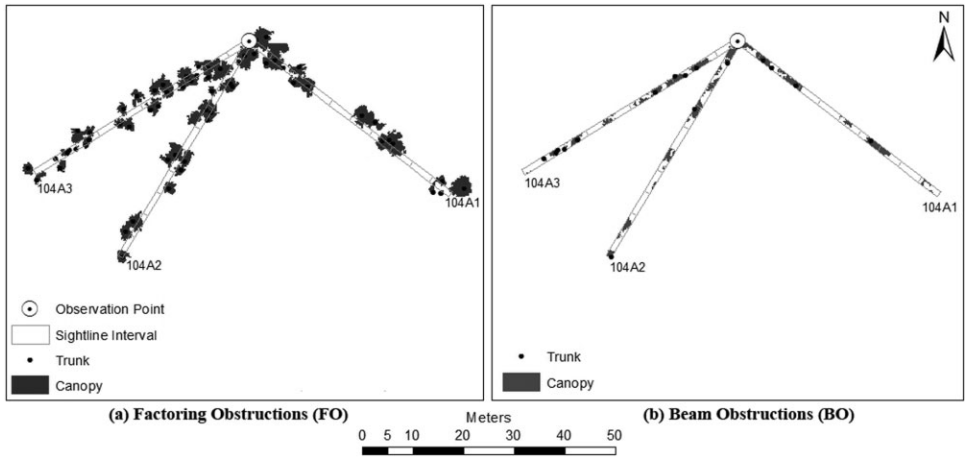


**Figure 2** Comparison of trunk and canopy extraction for plot 104A: (a) Canopies and subsequent trunks intersecting the 1 $m^2$ wide sightline beam were selected as factoring obstructions (FO); and (b) Vegetation instances inside the beam were quantified as beam obstructions (BO)

down perspective, each 1 m wide sightline was cut from the horizontal disk, producing a sightline "beam" of TLS data with a height and width of 1 m that extended from the scanner location out to 50 m. The process was repeated for each sightline corresponding in the TLS scans, resulting in 12 sightline "beams" of data. This cumulative total number of TLS points within the beam by a 5 m distance interval (referred to hereafter as 'cumulative TLS obstruction') was used for comparison with aerial LiDAR delineated tree characteristics and reference visibility values.

### *2.5 Identification of Vegetation Obstruction Factors*

Intersection locations between sightlines and vegetation data delineated from aerial LiDAR were used to identify which canopy and trunk obstructions were potential visibility obstructions. Two different methods of identifying vegetation data were used, both using a 1 $m^2$ sightline "beam" drawn from observation point to end point, corresponding to reference visibility samples. The first method, referred to as Factoring Obstructions (FO), identified all tree canopies and subsequent trunks which intersected or fell within 20 cm of the sightline beam as potential obstruction factors. The second method, Beam Obstructions (BO), identified canopies and trunks that were only inside the confines of the sightline beam (Figure 2).

Obstructions were delineated using the two methods to account for the difficulty of aerial LiDAR to detect subcanopy tree elements relevant to the sightline beam. The FO method sought to capitalize on the perspective of aerial LiDAR, and the tree delineation algorithm to accurately delineate the canopy area, even if the actual structure of lower tree elements was shadowed. The FO process surmised that a relationship between aerial LiDAR- and TLS-derived vegetation obstructions could potentially be established if allowance was made for canopy shadowing. Conversely, the BO process was implemented with the assumption that all canopy delineations were accurate relevant to subcanopy elements, and obstruction data identified within the confines of the sightline beam could be directly associated with TLS data. For comparison to reference and TLS datasets, canopy area and number of trunks were cumula-

 

tively totaled at each 5 m distance interval for both obstruction delineation methods. Collective vegetation totals at each interval were summed as accumulations over distance, to represent the compounding effect of vegetation obstructions on visibility.

### 2.6 Statistical Analysis

Vegetation factors delineated from aerial LiDAR and TLS were compared with reference visibility data at 5 m intervals to investigate the relationship between datasets. The rationale for analysis surmised that if a statistical association could be drawn between remotely sensed data and visibility, this information could be leveraged for creating a vegetation obstruction metric for modeling visibility. Specifically, a finite scale corresponding to the 1 $m^2$ sightline target was used to compare aerial LiDAR and TLS derived obstructions with each other, and with reference visibility. All statistical analyses were performed using IBM SPSS® Statistics Version 20 (Armonk, NY).

Spearman rank correlations (r values) were used to compare cumulative LiDAR and TLS-derived obstructions with reference visibility. Analysis of aerial LiDAR derived data was performed on FO derived beams and trunks and BO derived beams and trunks. Data were isolated into 5 m distance intervals, with 45 samples utilized for each correlation (n = 45). Analysis of TLS derived data was performed for 12 sightlines having corresponding obstruction and reference visibility data (n = 12). TLS points were tallied as obstructions cumulatively at each distance interval and compared directly to target visibility values.

The interplay between obstructions and visibility was assessed through linear regression, applied in two models. The first was a simple linear regression used to assess the relationship of aerial LiDAR as a predictor variable and TLS derived obstructions as the dependent variable. The second model was a multiple linear regression using aerial and terrestrial LiDAR obstructions as predictor variables and reference visibility as the dependent variable. Data from 12 sightlines containing TLS, aerial, and reference visibility data were grouped into 5 m distance intervals to ensure independence of predictor variables across all models (Table 1). Data were assessed for normality using Kolmogorov-Smirnov and Shapiro-Wilk tests. Cumulative TLS obstructions exhibited a non-normal distribution and were subsequently adjusted with a lognormal transform. Cumulative canopy area was normally distributed and remained unchanged. Reference visibility data revealed a non-normal distribution, and based on the proportional results of reference visibility calculations, an arcsine transformation was applied to achieve normality (McDonald 2009).

## 3 Results

### 3.1 LiDAR and TLS Visibility Correlations

Figure 3 shows the results from the Spearman rank correlation comparing cumulative TLS obstructions to calculated reference visibility at 5 m distance intervals. Results generally show a negative correlation caused by a decrease in visibility as TLS obstructions increased with distance. Despite rather high *r* values in some cases, only 5 and 10 m distance intervals show a significant correlation. Values at 35 and 50 m were unusually dispersed in both correlation and significance.

Table 2 shows the correlation between aerial LiDAR derived canopy area and trunk obstructions relative to reference visibility at 5 m distance intervals. Correlation was largely

 

**Table 1** Descriptive statistics for cumulative canopy area (Beam Obstruction (BO) isolation method), TLS obstructions, and reference visibility for data used in linear regression models (n = 12 for each distance interval)

| | Cumulative Canopy Area ($m^2$)[a] | | Cumulative TLS Obstructions[b] | | Reference Visibility (%)[c] | |
|---|---|---|---|---|---|---|
| Distance (m) | Mean | Std. Deviation | Mean | Std. Deviation | Mean | Std. Deviation |
| **5** | 2.8 | 2.5 | 5.49 | 5.92 | 1.32 | 0.33 |
| **10** | 5.7 | 3.5 | 9.87 | 3.62 | 1.04 | 0.41 |
| **15** | 8.5 | 4.2 | 10.85 | 1.75 | 0.92 | 0.45 |
| **20** | 10.5 | 4.5 | 10.97 | 1.55 | 0.86 | 0.43 |
| **25** | 12.5 | 4.4 | 11.11 | 1.31 | 0.76 | 0.37 |
| **30** | 15.6 | 5.9 | 11.13 | 1.29 | 0.68 | 0.28 |
| **35** | 17.6 | 6.0 | 11.14 | 1.29 | 0.60 | 0.23 |
| **40** | 19.7 | 7.4 | 11.15 | 1.29 | 0.58 | 0.28 |
| **45** | 22.0 | 7.8 | 11.16 | 1.27 | 0.50 | 0.30 |
| **50** | 24.0 | 8.6 | 11.17 | 1.26 | 0.46 | 0.30 |

a: Untransformed Cumulative Canopy Area, BO isolation method
b: Cumulative TLS obstructions, lognormal transform
c: Reference visibility, arcsine transform

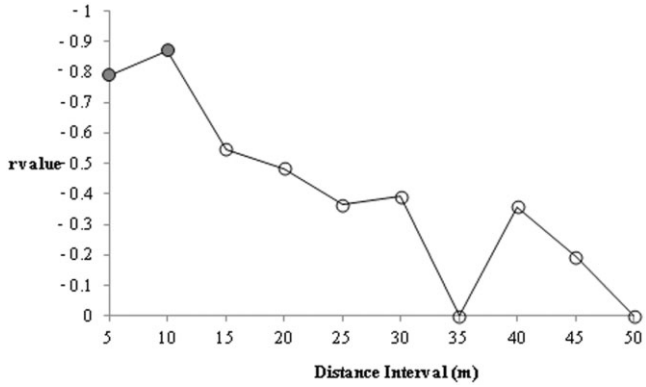


**Figure 3** Spearman rank correlation (r) between TLS and reference visibility at 5 m distance intervals (n = 12). Values at 5 and 10 m (grey circles) were significant (p = 0.05)

negative, reflecting an expected decrease in visibility as obstructions accumulate along the sightline path. Comparison between trunk and canopy across both FO and BO isolation methods shows that canopy area provides a better and more significant association with reference visibility than trunks, although both associations are relatively weak. FO and BO isolation method comparison is similar for canopy area, with trunks showing a somewhat better, however non-significant, correlation of trunk obstruction association with visibility.

 

**Table 2** Spearman rank correlation (*r*) results of airborne LiDAR derived Factoring Obstructions (FO) and Beam Obstructions (BO) canopy and trunk factors compared to reference visibility (n = 45). *r* values marked with asterisk (*) are significant at $p = 0.05$

| | FO | | BO | |
|---|---|---|---|---|
| Distance (m) | $r_{trunks}$ | $r_{canopy}$ | $r_{trunks}$ | $r_{canopy}$ |
| 5 | –0.44* | –0.45* | –0.19 | –0.36* |
| 10 | –0.29* | –0.41* | –0.03 | –0.47* |
| 15 | –0.24 | –0.31* | –0.26 | –0.28 |
| 20 | –0.34* | –0.32* | –0.32* | –0.33* |
| 25 | –0.18 | –0.20 | –0.38* | –0.30* |
| 30 | –0.19 | –0.30* | –0.17 | –0.33* |
| 35 | –0.20 | –0.24 | 0.04 | –0.28 |
| 40 | –0.16 | –0.35* | 0.21 | –0.29* |
| 45 | –0.14 | –0.27 | –0.14 | –0.22 |
| 50 | –0.10 | –0.25 | 0.13 | –0.29 |
| *Mean* | *–0.23* | *–0.31* | *–0.11* | *–0.31* |

### *3.2 Regression Results*

Comparison of aerial LiDAR and TLS obstructions was performed with a simple linear regression using aerial LiDAR derived beam obstructions as predictor variables and lognormal transformed TLS obstructions as dependent variables (Table 3). $R^2$ values were good at shorter distances, gradually declining with distance. Analysis of variance (ANOVA) conducted in conjunction with the regression shows significance at 0.05 for 5 and 10 m, but also deteriorates with distance. An anomaly is present at 30 m in the otherwise constant pattern of decline in both $R^2$ and significance. Root mean square error (RMSE) is reported as log transformed TLS obstruction values and is generally consistent across all distance intervals.

The final analysis utilized a multiple linear regression model with TLS and aerial LiDAR derived canopy area obstructions as predictor variables and reference visibility as the dependent variable (Table 4). $R^2$ values were higher at closer intervals, with a gradual decline over distance. ANOVA reflects that only results from the 10 m interval showed a significant relationship ($p = 0.05$).

## 4 Discussion

General results present a confounding association between reference visibility and LiDAR derived vegetation obstructions. The results could be attributed to several factors within the experiment design and process; however, attempting to quantify lodgepole pine structure at such a discrete level was probably the most significant contributor to the lack of positive results. The degree of variability of tree growth characteristics and the complexity of canopy and subcanopy structure relative to a single 1 $m^2$ beam of visibility proved extremely difficult to detect and model with the study datasets. A larger (than 1 $m^2$) sightline beam may provide more positive results allowing better representation of sub-canopy variability in the visibility

 

**Table 3** Linear regression results using aerial LiDAR derived obstructions as predictor and TLS obstructions as dependent variables. Results are reported in log transformed values for TLS data (n = 12)

| Distance (m) | $R^2$ | RMSE | Sig. | β |
|---|---|---|---|---|
| **5** | 0.68 | 1.40 | 0.04 | 0.82 |
| **10** | 0.67 | 1.18 | 0.00 | 0.82 |
| **15** | 0.51 | 1.29 | 0.09 | 0.71 |
| **20** | 0.31 | 1.35 | 0.06 | 0.56 |
| **25** | 0.26 | 1.18 | 0.09 | 0.51 |
| **30** | 0.37 | 1.07 | 0.04 | 0.61 |
| **35** | 0.28 | 1.15 | 0.08 | 0.53 |
| **40** | 0.26 | 1.16 | 0.09 | 0.51 |
| **45** | 0.17 | 1.21 | 0.18 | 0.42 |
| **50** | 0.12 | 1.25 | 0.28 | 0.34 |

RMSE: Root Mean Square Error
Sig: ANOVA significance
β: Standardized beam obstructions canopy area coefficient

**Table 4** Multiple linear regression using cumulative TLS obstructions and aerial LiDAR derived canopy area obstructions as predictor variables and reference visibility as the dependent variable (n = 12). Reference visibility and TLS obstruction values are arcsine and lognormal transformed respectively

| Distance (m) | $R^2$ | RMSE | Sig. | $\beta_t$ | $\beta_a$ |
|---|---|---|---|---|---|
| **5** | 0.42 | 0.28 | 0.09 | –0.70 | 0.10 |
| **10** | 0.46 | 0.30 | 0.03 | –0.25 | –0.55 |
| **15** | 0.46 | 0.36 | 0.06 | –0.93 | 0.46 |
| **20** | 0.35 | 0.39 | 0.14 | –0.71 | 0.33 |
| **25** | 0.14 | 0.38 | 0.51 | –0.40 | 0.35 |
| **30** | 0.22 | 0.27 | 0.33 | –0.58 | 0.46 |
| **35** | 0.20 | 0.23 | 0.37 | –0.42 | 0.49 |
| **40** | 0.13 | 0.28 | 0.53 | –0.42 | 0.20 |
| **45** | 0.04 | 0.32 | 0.82 | –0.07 | –0.17 |
| **50** | 0.03 | 0.33 | 0.86 | 0.08 | –0.19 |

$\beta_t$ Standardized TLS coefficient
$\beta_a$ Standardized canopy area coefficient

analysis. An adjusted method for establishing reference visibility values, potentially using a larger target or less discrete process, could be better suited for assessing subcanopy structure.

### *4.1 TLS-derived Obstructions Versus Reference Visibility*

Correlation between cumulative target obstructions derived from TLS and digital photographs was promising. Since sensor vantage points were kept constant using GPS delineated observa-

 


**Figure 4** Obstruction comparison between digital photography and TLS imagery of 1 $m^2$ target in plot 104A1 at 10 m: (a) High resolution of digital photography enables delineation of branch and needle obstructions (trunk and branches are colored black in image); and (b) TLS data produces a coarser representation of obstructions

tion points with a relatively constant height, correlation between datasets at 5 m intervals was expected to be comparatively good, and results were consistent with predictions. Differences in sightline perspective caused by placement error between the digital camera and the TLS sensor are attributable to some dataset variability. Sensor capability, however, is almost certainly a more significant factor in dataset differences, as the resolution of the digital photograph is better than the active TLS sensor. TLS pulses are emitted, returned, and assembled by the sensor in a three-dimensional array with spacing between pulses mechanically controlled by the sensor configuration at emission. The Leica ScanStation C10 sensor emits laser pulses with a beam diameter of 4.5 mm and with an array resolution of <1 mm. While relatively small at short distances, both the beam diameter of the laser and the spacing of the array of pulses diverge as distance from the scanner increases (Lichti et al. 2002). Consequently, target obstructions such as branches and needles, which allow some target visibility in digital photographs, can be overestimated by TLS. Reflections of the TLS beams are interpreted as full obstructions in the point cloud array, when in reality they are only partial obstructions (Lichti 2004). Finally, unlike a digital camera, TLS scanners collect data by rotating slowly, allowing vegetation movement due to wind to have an impact during data collection. Figure 4 depicts the resolution disparity between digital photography and TLS for calculating proportions of target obstruction.

### *4.2 Aerial LiDAR Derived Obstructions Versus Reference Visibility*

A weak negative correlation between aerial LiDAR derived obstructions and reference visibility for potential association of canopy area or trunks as vision obstructions was observed (Table 2). This can be attributed to the inability of aerial LiDAR to accurately detect all subcanopy vegetation factors influential to visibility. Comparison between the BO and FO methods used to isolate tree elements relative to the sightline beam showed that the FO method produced slightly better correlation with the trunks, but the difference between the two methods was not significant.

The weak relationship between LiDAR-derived trunk and canopy data, and reference visibility, can largely be credited to the canopy shadowing limitation of aerial LiDAR, in a

 

lodgepole pine ecosystem (Zimble et al. 2003). In addition, errors in vegetation structure delineation, particularly trunk locations, can be attributed to both the forest structure and the tree crown delineation process. Lodgepole pine growth is characterized by dense stands, uneven intra-stand heights, and leaning trees (Steele et al. 1981), which makes delineation and location of individual trees challenging. Processing of LiDAR point cloud data, conversion to a raster and subsequent delineation of trunks and canopies further introduces error through conversion of continuous detail in the digitization process and subsequent feature loss.

### *4.3 Integration of Aerial LiDAR and TLS for Prediction of Visibility*

The scale of delineation is a critical element for interpretation of aerial LiDAR characterization of forest structure. Translation of relatively coarse data with a non-optimal perspective to discrete elements is realistically ineffective, as demonstrated by the weak correlation between aerial derived tree characteristics and visibility data. As a solution, augmenting aerial LiDAR delineated canopies with TLS data to estimate subcanopy elements may be possible for short distances from the terrestrial sensor, as depicted in Table 3. The small sample size probably introduces error and bias into results, which may be the cause of the anomaly of $R^2$ and significance values at the 30 m interval.

TLS obstruction at distances greater than 10 m showed an unreliable association with aerial derived canopies, potentially caused by shadowing of data in the lateral plane, similar to canopy shadowing in aerial LiDAR. A single scan of data does not produce a reliable inventory of vegetation elements beyond the first obstructions, corresponding to the decrease in both $R^2$ and significance of results beyond 10 m. Modeling of forest structure with TLS can utilize scanning from multiple locations to minimize this obstruction shadowing (Côté et al. 2011, Henning and Radtke 2006), but this may entail more time and effort for data collection and processing. Instead of 3D structural information delineated from one side of a tree for a single scan, multiple scanning can be leveraged to provide a full 360° representation of the entire tree canopy and trunk, which increases the density and coverage of data that can potentially minimize the lateral shadowing effect and make TLS data more useful for longer distance visibility modeling. Where only a single scan TLS data is available, such as in the present study, integration with aerial LiDAR can offset some of the lateral shadowing effects of TLS for visibility modeling, especially across large areas.

Finally, aerial LiDAR derived, BO isolated canopy and TLS obstructions as predictor variables were regressed against reference visibility. A fair to poor association was found between LiDAR derived obstructions and visibility (Table 4). $R^2$ and significance results declined with distance, consistent with previous analyses incorporating TLS, and reflected the decrease of effectiveness of single scan TLS data caused by lateral obstruction shadowing.

## 5 Conclusions

Laser scanning datasets from both aerial and terrestrial sensors are complementary in that they provide a wealth of forest information from different viewing perspectives. This study showed that, while aerial LiDAR derived canopy and trunk obstructions were not effective in lateral visibility analysis, TLS-derived subcanopy obstructions has excellent potential for visibility modeling. Furthermore, this study is one of the early attempts to integrate data from both aerial LiDAR and TLS sensors for visibility obstruction modeling. The fusion of data from the two sensors was relatively ineffective for short-range visibility in a forested environment, as

 

presented here. These results, however, do not diminish the potential for terrestrial-sensed subcanopy metrics for augmentation of large amounts of aerial LiDAR data to significantly improve models of forest structure. While this study used a relatively homogenous lodgepole pine stand with minimal underbrush to test the model, future studies comparing the results to more complex vegetation with different structure and composition are recommended. Subtle LiDAR processing improvements, including more accurate tree delineation through higher point density aerial data, combined with better vegetation quantification processes for TLS data such as thresholding and octree filtering, could drastically advance the feasibility and accuracy of data integration. The discrimination of branches and trunks can be refined and automated for application in viewshed modeling by using TLS sensors that are able to seamlessly record more calibrated information, such as intensity and reflectance. In addition, using full waveform data from a terrestrial or airborne scanner with a higher penetration and resolving capability through leaves and branches might improve the visibility model, especially at a longer range (>10 m). While this integration of data is pertinent to visibility models, as was the focus of our research, benefits extend into several applications, including estimation of biomass and carbon sequestration, wildlife habitat monitoring, wildfire fuel quantification, among others.

## References


Bartie P, Reitsma F, Kingham S, and Mills S 2011 Incorporating vegetation into visual exposure modeling in urban environments. *International Journal of Geographic Information Science* 25: 851–68

Böhm J and Haala N 2005 Efficient integration of aerial and terrestrial laser data for virtual city modeling using lasermaps. In *Proceedings of the 2005 ISPRS WG III/3, III/4, V/3 Workshop on Laser Scanning*, Enschede, The Netherlands: 192–7

Chasmer L, Hopkinson C, and Treitz P 2006 Investigating laser pulse penetration through a conifer canopy by integrating airborne and terrestrial LiDAR. *Canadian Journal of Remote Sensing* 32: 116–25

Chen Q, Baldocchi D, Gong P, and Kelly M 2006 Isolating individual trees in a Savanna woodland using small footprint LiDAR data. *Photogrammetric Engineering and Remote Sensing* 72: 923–32

Coops N, Hilker T, Wulder M, St-Onge B, Siggins A, Newhnam G, Siggins A, and Trofymow J A 2007 Estimating canopy structure of Douglas-fir forest stands from discrete-return LiDAR. *Trees – Structure and Function* 21: 295–310

Côté JF, Fournier R A, and Egli R 2011 An architectural model of trees to estimate forest structural attributes using terrestrial LiDAR. *Environmental Modelling and Software* 26: 761–77

Dean D 1997 Improving the accuracy of forest viewsheds using triangulated networks and the visual permeability method. *Canadian Journal of Forest Research* 27: 969–77

Fisher P F 1992 First experiments in viewshed uncertainty: Simulating fuzzy viewsheds. *Photogrammetric Engineering and Remote Sensing* 58: 345–52

Hall S A, Burke I C, Box D O, Kaufmann M R, and Stoker J M 2005 Estimating stand structure using discrete-return LiDAR: An example from low density, fire prone ponderosa pine forests. *Forest Ecology and Management* 208: 189–209

Henning J G and Radtke P J 2006 Ground-based laser imaging for assessing three-dimensional forest canopy structure. *Photogrammetric Engineering and Remote Sensing* 72: 1349–58

Hyyppa J, Hyyppa H, Litkey P, Yu X, Haggren H, and Ronnholm P 2004 Algorithms and methods of airborne laser scanning for forest measurements. *International Archives of Photogrammetry, Remote Sensing, and Spatial Information Sciences* 36(8/W2): 82–9

Ke Y and Quackenbush L J 2008 Comparison of individual tree crown detection and delineation methods. In *Proceedings of the 2008 American Society of Photogrammetry and Remote Sensing Annual Conference*, Portland, Oregon

Kwak D A, Lee W K, Lee J H, Biging G S, and Gong P 2007 Detection of individual trees and estimation of tree height using LiDAR data. *Journal of Forest Research* 12: 425–34

Lefsky M A, Cohen W B, Parker G G, and Harding D J 2002 LiDAR remote sensing for ecosystem studies. *Bioscience* 52: 19–30

Lefsky M A, Hudak A T, Cohen W B, and Acker S A 2005 Patterns of covariance between forest stand and canopy structure in the Pacific Northwest. *Remote Sensing of the Environment* 95: 517–31


 

Lichti D 2004 A resolution measure for terrestrial laser scanners. *International Archives of the Photogrammetry, Remote Sensing and Spatial Information Sciences* 34(B5): 552–8

Lichti D D, Gordon S J, and Stewart M P 2002 Ground based laser scanners: Operation systems and applications. *Geomatica* 56: 21–33

Liu L, Zhang L, Chen C, and Hong C 2008 An improved LoS method for implementing visibility analysis of 3D complex landscapes. In *Proceedings of the International Conference on Computer Science and Software Engineering*, Wuhan, China: 874–7

Llobera M 2007 Modeling visibility through vegetation. *International Journal of Geographic Information Science* 21: 799–810

McDonald J 2009 *Handbook of Biological Statistics*. Baltimore, MD, Spark-House

Moskal L M, Erdody T, Kato A, Richardson J, Zheng G, and Briggs D 2009 LiDAR applications in precision forestry. In *Proceedings of the 2009 Silvilaser Conference*, College Station, Texas

Murgoitio J J 2012 Visibility modeling with LiDAR derived forest variables. Unpublished M.S. Thesis, Idaho State University

Murgoitio J J, Shrestha R, Glenn N F, and Spaete L P 2013 Improved visibility calculations with trunk obstruction modeling from aerial LiDAR. *International Journal of Geographical Information Science* 27: in press

Ni-Meister W, Jupp D L, and Dubayah R 2001 Modeling LiDAR waveforms in heterogeneous and discrete canopies. *IEEE Transactions on Geoscience and Remote Sensing* 39: 1943–58

Ogburn D E 2006 Assessing the level of visibility of cultural objects in past landscapes. *Journal of Archaeological Science* 33: 405–13

Persson A, Homgren J, and Soderman U 2002 Detecting and measuring individual trees using and airborne laser scanner. *Photogrammetric Engineering and Remote Sensing* 58: 925–32

Popescu S C and Wynne R H 2004 Seeing the trees in the forest: Using LiDAR and multispectral data fusion with local filtering and variable window size for estimating tree height. *Photogrammatic Engineering and Remote Sensing* 70: 589–604

Richardson J J, Moskal L M, and Kim S H 2009 Modeling approaches to estimate effective leaf area index from aerial discrete-return LiDAR. *Agriculture and Forest Meteorology* 149: 1152–60

Standford C, Williams P, Sanderson D, Pash K, and Lohmeyer D 2003 Enhanced line-of-sight modeling and associated scenario development issues. Edinburgh, Australia, Defence Science and Technology Organization (DSTO) External Publications

Steele R, Pfister R D, Ryker R A, and Kittams J A 1981 *Forest Habitat Types of Central Idaho*. Moscow, ID, U.S. Forest Service

Streutker D and Glenn N 2006 LiDAR measurement of sagebrush steppe vegetation heights. *Remote Sensing of Environment* 102: 135–45

Wang Y, Weinacker H, and Koch B 2008 A LiDAR point cloud based procedure for vertical canopy structure analysis and 3D single tree modelling in forest. *Sensors* 8: 3938–51

Zimble D A, Evans D L, Carlson G C, Parker R C, Grado S C, and Gerard P D 2003 Characterizing vertical forest structure using small-footprint airborne LiDAR. *Remote Sensing of the Environment* 87: 171–82

 